ACS APPLIED MATERIALS & INTERFACES

Research Article

www.acsami.org

Self-Assembled TiO_2 Nanospheres By Using a Biopolymer as a Template and Its Optoelectronic Application

Saikat Dutta,[†] Astam K. Patra,[‡] Sudipta De,[†] Asim Bhaumik,*[,‡] and Basudeb Saha*[,†]

[†]Laboratory of Catalysis, Department of Chemistry, University of Delhi, North Campus, Delhi-110 007, Delhi, India

[‡]Department of Materials Science, Indian Association for the Cultivation of Science, Jadavpur, Kolkata-700032, India

Supporting Information

ABSTRACT: Self-assembled TiO_2 nanoparticulate materials with well-defined spherical morphologies were synthesized by using a biopolymer sodium alginate as a template under different synthesis conditions. Powder X-ray diffraction (XRD), transmission electron microscopy (TEM), and scanning electron microscopy (SEM) techniques were used to characterize the TiO_2 nanoparticles. N_2 sorption analysis revealed the moderately good surface area (124.0 m^2 g^{-1}) and pore volume (0.44 cm^3 g^{-1}) of these TiO_2 nanoparticles. The biopolymer templating pathway leads to good-quality self-assembled TiO_2 nanoparticles with dimensions of ca. 10−12 nm within the synthesis temperature range of 0−60 °C. These porous TiO_2 nanomaterials showed high photogenerated current in the presence of a dye (Rose Bengal), used as a sensitizer for several photo on/off cycles.

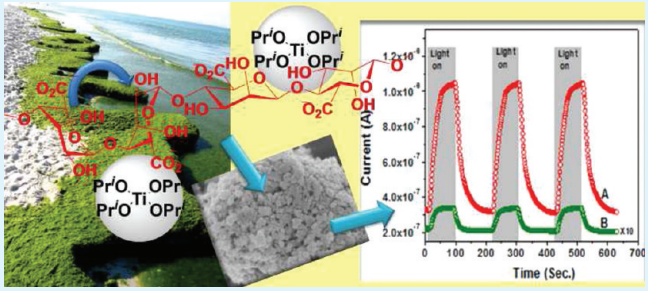

KEYWORDS: *self-assembly of nanoparticles, photoconductivity, biopolymer templating, mesoporous materials, TiO_2*

INTRODUCTION

Titanium dioxide (TiO_2) has excellent chemicophysical properties, and unique applications of this material have been found in several emerging areas, including photocatalysis, gas sensors, solar cells, and Li-ion batteries.[1−5] Extensive research efforts on controlling the microstructure and morphology of TiO_2 to achieve novel and enhanced properties have been witnessed. Furthermore, porous TiO_2 nanospheres have attracted great interest in this context, because of their high surface area, surface permeability, and light-trapping effect.[6−9] In the recent years, TiO_2-based materials have been applied extensively in environmental,[10] sensing,[11] photocatalytic,[12−14] and optoelectronic applications.[15,16] However, the major drawbacks, such as low surface area and high band gap, often restricted TiO_2 nanostructured material for suitable applications. The surface area of TiO_2-based materials can be enhanced significantly by introducing nanoscale porosity at its surface. The supramolecular assembly of ionic or neutral surfactants has been conventionally employed as a template or structure directing agent to design mesoporous materials.[17−19] Moreover, TiO_2 material with desired mesoporosity can be prepared by templating with various agents such as dendrimers,[20] polymers,[21] and aromatic acid.[22] In addition, hierarchically anatase mesoporous/nanoporous S- and C-doped TiO_2[23] and solvothermal method derived TiO_2 microspheres[24] have been recently reported for their promising photocatalytic activity.

TiO_2-based nanostructured materials have been prepared using various synthetic strategies, including the soft-templating pathway, e.g., surfactant micelles as templates[25,26] and also hard templating.[27] Generally, the templating method of preparation of titania nanoparticles involves calcinations at high temperatures to remove the template and leave behind pores in the TiO_2 matrix. During the calcination process, sintering and crystallization also occurs, which can cause collapse of the nanostructure, resulting in a significant loss in surface area. Thus, proper choice of the template molecule and its efficient removal from the surface TiO_2 matrix are highly desirable to achieve TiO_2-based nanostructured materials. Controlled growth of nanostructured TiO_2 using a templating agent that contains carboxylate groups in aromatic and amino acids[22,28] prompted us to investigate the structure directing ability of biopolymer sodium alginate for the controlled growth of the self-assembled TiO_2 crystallites in nanoscale dimension.

Recently, biopolymers have been shown to exert a remarkable degree of control over the nucleation and growth of crystalline metal oxides.[29] Alginate, for example, is the structural biopolymer found in seaweed and contains blocks of guluronate monomers (Scheme 1) that are readily cross-linked by strong electrostatic bonds to multivalent metal cations. High thermal stability and extended gel network structure in aqueous media made biopolymers capable of maintaining the preorganized dispersion of metal cations to relatively high temperature, i.e., influence the nucleation and growth of crystalline phases.[30]

On the other hand, since ultraviolet (UV) irradiation at the semiconductor surface is energetically unfavorable, significant research has been directed toward extending the absorption

Received: December 12, 2011
Accepted: February 15, 2012
Published: February 15, 2012

Scheme 1. Structure of Alginate Containing Guluronate (G) and Mannuronate (M) Epimers, and Schematic Diagram for the Synthesis of TiO_2 Nanospheres from Titanium Isopropoxide, Using Alginate As a Template

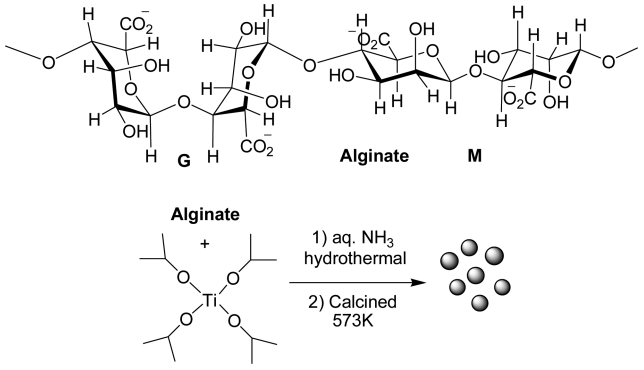

edge of TiO_2-based nanostructured materials toward the visible-light (Vis) region of the spectrum by doping TiO_2 with metallic,[31] nonmetallic,[32] or organic species[33] at the surface or in the crystal lattice. Electron injection from a photosensitizer molecule trapped inside the pores of the semiconductor surface can facilitate its Vis-induced generation of a photocurrent.[34] Recent examples of TiO_2-based photoconductors are graphene-TiO_2 material[35] and frequency-dependent photoconductivity in a TiO_2 nanotube.[36]

Metal binding and structure directing capacity of the biopolymer alginate, with its ability to reduce metal salts to nanoparticles of desired structures, is something yet to be explored, except a recent work on fabrication of titania microspheres using alginate microdroplets on an oil/hydrogen interface.[37] Since the biopolymer alginate forms an extended gel network in aqueous medium and metal cations dispersed through the structure upon heating, preorganization of metal cations within the polymer gel may lead to constrained nucleation of metal oxide nanoparticles. Another advantage of using alginate as template for nanostructured materials synthesis is a minimum quantity of templating agent would be sufficient for the process, instead of using a stoichimetric quantity with metal precursors, because of the extended polymeric network structure. Herein, we report a strategic synthesis of porous TiO_2 nanospheres using alginate biopolymer as the structure directing agent. In the synthesis reaction, primarily TiO_2 nanospheres with mesoscopic void spaces were produced through the hydrolysis of titanium isopropoxide in aqueous media under an alkali treatment method (Scheme 1). To illustrate the effect of the temperature during nucleation of the nanospheres, synthesis was also carried out at various temperatures: low temperature (0 °C), room temperature (25 °C), and at 60 °C. The TiO_2 materials were fully characterized by using scanning electron microscopy (SEM), high-resolution transmission electron microscopy (HR-TEM), and powder XRD. The surface area and pore volume was analyzed using a N_2-sorption technique. Pore size was analyzed by using nonlocal density functional theory (NLDFT) on the sorption isotherms. The prospects of the photochemical application of the mesoporous TiO_2 nanospheres have been elucidated by using Rose Bengal (RB) dye as a photosensitizer in the dye–TiO_2 nanocomposites and subsequent high photocurrent generation.

EXPERIMENTAL SECTION

Sodium alginate and titanium isopropoxide were supplied by Sigma–Aldrich and were used without further purification. Ammonia solution (25%) were supplied by Spectrochem (India). Unless otherwise stated, distilled water was used as aqueous phase.

A field-emission scanning electron microscopy (FESEM) system (JEOL, Model JEM 6700F) was used to determine the particle morphology of the TiO_2 nanoparticles. High-resolution transmission electron microscopy (HR-TEM) images were recorded on a JEOL DATUM system (Model JEM1011). Powder X-ray diffraction (XRD) patterns of the TiO_2 samples were recorded on a Bruker D-8 Advance diffractometer operated at a voltage of 40 kV and current of 40 mA, using Cu Kα (λ = 0.15406 nM) radiation. Nitrogen sorption isotherms were obtained using a Beckmann Coulter model SA3100 surface area analyzer at 77 K. Prior to the measurement, the samples were degassed at 393 K for 12 h. The DC current between the two electrodes was measured using a Keithley source meter (Model 2420). The photocurrent was measured by illuminating with white light from a 150-W xenon lamp source (Newport Corp., USA; Model 69907).

Preparation of TiO_2 from Titanium Isopropoxide and Sodium Alginate. Sodium alginate (1.0 g) was dissolved in 300 mL water by stirring at 80 °C. To this solution, titanium isopropoxide (14 mL) was added at room temperature and the pH of the reaction mixture was adjusted to 10.0 via the dropwise addition of an aqueous ammonia (25%) solution and rapid stirring at room temperature. The reaction mixture was then divided into three parts in equal volume and separately stored in a freezer at (0 °C), at room temperature and at 60 °C in hot oven for aging for 24 h. The resultant solids were collected by repeated centrifugation (8000 rpm, 10 min) and washing with distilled water. The solid was dried in oven at 80 °C for overnight (8 h) and then calcined at 300 °C in furnace for 4 h. TiO_2 materials prepared at room temperature, 0 °C, and under hydrothermal (60 °C) condition were designated as TiO_2–R, TiO_2–F, and TiO_2–H, respectively. In another experiment, sodium alginate was not used in the synthesis medium and TiO_2 material was synthesized in the same procedure maintaining the pH = 10 only by using ammonia solution. The detail of the synthesis procedure was described in the Supporting Information.

Photoconductivity Measurements with TiO_2. For the electrical measurements, first, pellets of the TiO_2–H sample (1 cm in diameter) were prepared and two gold electrodes (of ca. 50 nm thickness) were thermally evaporated on each pellet in the circular form with a diameter of 2 mm through a shadow mask at a separation of 4 mm.

RESULTS AND DISCUSSIONS

The wide-angle XRD patterns of the TiO_2 nanoparticles are shown in Figure 1a and Figure S1 in the Supporting Information . Observed crystalline planes agree very well with the anatase TiO_2. The crystalline planes corresponding to the peaks for anatase TiO_2 have been indexed in Figure 1a. All calcined samples show major peaks at 2θ values of 25.3°, 37.8°, 48.0°, 53.7°, 54.9°, and 62.5°, which correspond to anatase (101), (004), (200), (105), (211), and (204) crystal planes (JCPDS File Card No. 21-1272).[22] The wide-angle powder XRD results revealed that the alginate templating method and the nontemplating method produced highly stable and crystalline TiO_2 nanoparticles and nanospheres, respectively. A representative TEM image of the mesoporous TiO_2 nanoparticles (TiO_2–F) calcined at 300 °C is shown in Figure 1b, and the HR-TEM images are shown in Figures 1c and 1d. As seen in these figures, a spherical tiny TiO_2 nanoparticle with dimensions of 10–15 nm is assembled by forming a self-aggregated (loose assembly) nanostructure and the (101) plane is quite clear in these image. The selected area electron diffraction (SAED) pattern shown in Figure 1e suggested the diffraction spots for crystalline anatase TiO_2.

Further evidence in support of the self-assembled TiO_2 nanoparticles for samples prepared hydrothermally and at room temperature is obtained from their respective FE SEM images (see Figures 2a and 2b). Both samples are composed of uniform tiny spherical nanoparticles 10–15 nm in size (see

dx.doi.org/10.1021/am201759w | ACS Appl. Mater. Interfaces 2012, 4, 1560–1564

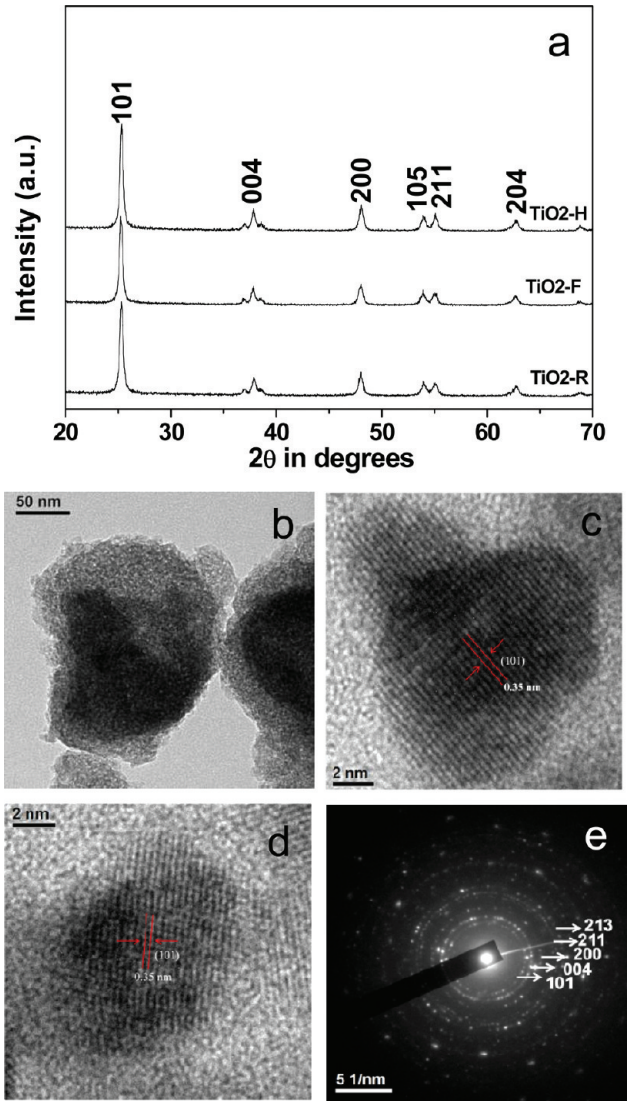

Figure 1. (a) XRD profile of the TiO_2 samples (TiO_2–R, TiO_2–F, TiO_2–H) with indexed peaks. (b) HR-TEM image of typical nanostructure of TiO_2–F. (c and d) HR-TEM image of typical nanostructure of TiO_2–F, showing (101) crystalline planes. (e) Selected-area electron diffraction (SAED) pattern of the calcined mesoporous TiO_2–F.

Figures 2a and 2b), and there are interparticle voids ca. 10 nm in size. However, when the TiO_2 materials were synthesized in the absence of sodium alginate, the size of the particles increased considerably. The FE SEM image in the Supporting Information (Figure S2) shows that the sample is composed of large nanospheres 100–200 nm in size. Li et al. also observed similar particle morphology in the hydrothermally synthesized TiO_2 in the presence of ammonia.[38] This experiment explores the templating role of the sodium alginate biopolymer, which controls the particle size of the TiO_2 materials.

The N_2 adsorption/desorption isotherms of the TiO_2 materials obtained by using sodium alginate as the template are shown in Figure 3. Isotherms for TiO_2–H, TiO_2–R (Figure 3), and TiO_2–F (see the Supporting Information and Figure S1) could be classified as type IV isotherms corresponding to the mesoporous materials, based on their behavior at high partial pressures P/P_0. Hydrothermally prepared TiO_2–H material shows a high surface area among them. The BET surface areas

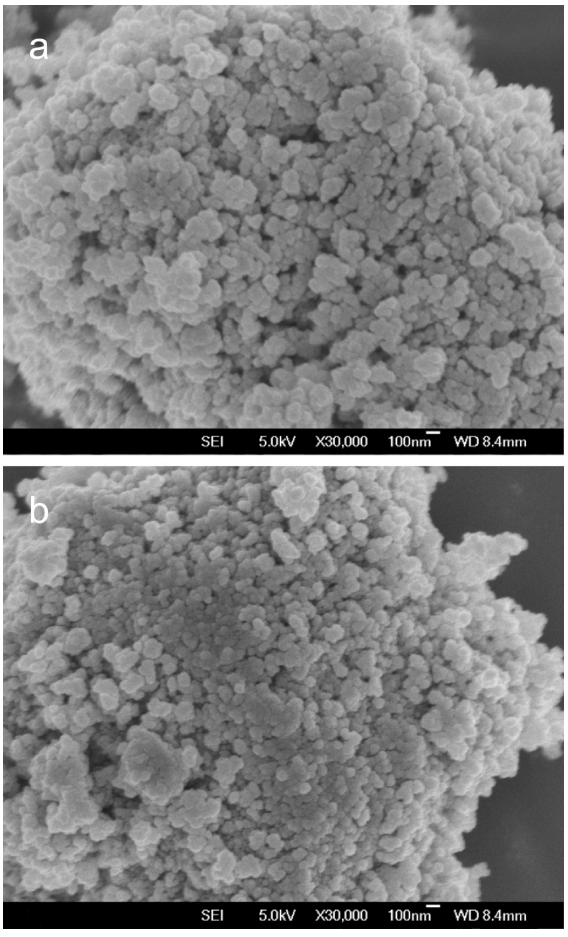

Figure 2. FE-SEM image of calcined (300 °C) mesoporous TiO_2 samples prepared under hydrothermal condition and at low temperature: (a) TiO_2–H and (b) TiO_2–F.

of TiO_2–H, TiO_2–R, and TiO_2–F samples were 124.0 $m^2\ g^{-1}$, 74.02 $m^2\ g^{-1}$, and 50.21 $m^2\ g^{-1}$, respectively. The pore volumes of these samples were 0.44 $cm^3\ g^{-1}$, 0.21 $cm^3\ g^{-1}$, and 0.44 $cm^3\ g^{-1}$, respectively. In the absence of an alginate template, when the synthesis was carried out in the presence of ammonia alone, the TiO_2 materials have comparatively less surface area (35–60 $m^2\ g^{-1}$, as shown in Figure S4 and Table S11 in the Supporting Information) and very low pore volume. For the samples synthesized with templates, the isotherm gradually increased between a P/P_0 range of 0.05–0.70.[22] A large increase in the adsorption occurred at higher P/P_0 values (0.70–0.85), for all the samples. The pore size distributions of the samples, measured using the nonlocal density functional theory (NLDFT) method (using N_2 adsorption on silica as a reference), suggested that the TiO_2–H synthesized at 60 °C has a larger pore (ca. 11.68 nm; see Figure 3c) than TiO_2–R and TiO_2–F materials. TiO_2–F has an average pore dimension of ca. 9.2 nm. A similar decrease in the dimension of the pores with decreasing synthesis temperature was also observed for our TiO_2 nanoparticles synthesized by using sodium salicylate as a template.[22]

The calcined mesoporous TiO_2–H and Rose-Bengal (RB)-entrapped TiO_2–H–RB samples were kept in darkness for 12 h before the dark currents were measured. Linear dark current I–V characteristics, as shown in Figure 4A, suggested Ohmic behavior of the gold contacts in the samples. Furthermore, from Figure 4A, it is clear that the dark current is much higher for the

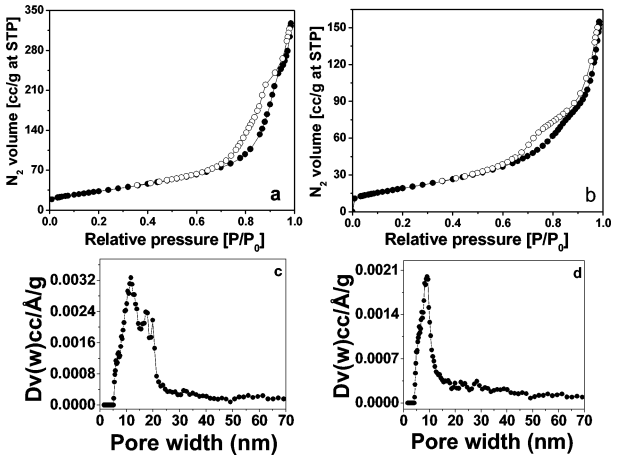

Figure 3. N_2 adsorption−desorption isotherm of (a) the calcined TiO_2−H and (b) TiO_2−R at 77 K ((●) adsorption and (○) desorption). Representative pore size distributions using the nonlocal density functional theory (NLDFT) method are shown in panels (c) and (d), for TiO_2−H and TiO_2−R respectively.

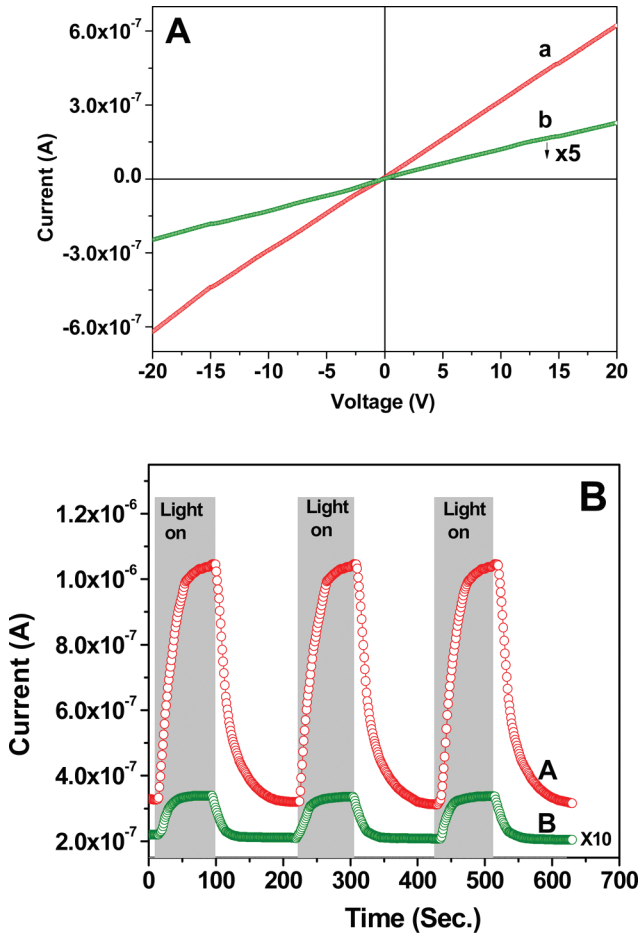

Figure 4. (A) Dark-current I−V plots of template-free TiO_2 (green line, b) and after impregnating rose bengal (RB) in mesoporous TiO_2 (red line, a). (B) The growth/decay of photocurrent with time over calcined TiO_2 (Green B) and RB-trapped TiO_2 (Red A) on white-light illumination. Light on/off points of these samples are shown in three cycles.

RB-entrapped mesoporous TiO_2, compared to that in the absence of the sensitizer. The dye molecule reduced the bandgap in TiO_2−H−RB, which could be due to ligand-to-metal charge transfer, and this could be very helpful for photocurrent generation, since, upon photoexcitation, the dye molecule can easily inject the electrons into the conduction band[22,39] of the self-assembled TiO_2 nanoparticles and, thus, electronic conduction could proceed smoothly. Figure 4B shows the photocurrent transients of dye-loaded and unloaded self-assembled TiO_2 nanoparticles with a 10 V bias. As soon as visible light is shone upon the samples, the current increases, suggesting that the samples are sensitive to the white light. The maximum current value after Vis illumination to the RB-entrapped TiO_2−H−RB sample reaches 1.05×10^{-6} A, while the value for the RB-free TiO_2 sample was only 5.06×10^{-8} A. The value of the photogenerated current ΔI (photocurrent minus dark current) for the RB-entrapped mesoporous TiO_2 sample is 0.74×10^{-6} A, whereas for RB-free TiO_2, it was only 3.27×10^{-8} A. This indicates a large change in the photocurrent generation, which is ∼22.6 times greater in the dye-doped composite, compared to the RB-free TiO_2. For a TiO_2−RB sample, upon illumination of light energy greater than of its bandgap, electron−hole pairs are generated at the porous surface. These photogenerated electrons then can easily be transferred from the conduction band of RB to the conduction band of TiO_2.[40] Thus, the RB dye acts as a Vis sensitizer. Furthermore, the higher surface area of these semiconductor nanoparticles could be responsible for higher photon-to-electron conversion efficiency.[41,42] Thus, this photoconductivity experiments suggested the tunneling of these electron−hole pairs through the self-assembled TiO_2 nanoparticles in the presence of the RB sensitizer, leading to a higher photogenerated current.

When compared with our previous results, a wide difference in surface area (118−326 $m^2\ g^{-1}$) was found for the titania materials synthesized at different temperatures using sodium salicylate as a template.[22] In the case of the alginate-templated mesoporous TiO_2 nanospheres, the surface area varied from 50 $m^2\ g^{-1}$ to 124 $m^2\ g^{-1}$ for the materials prepared in the temperature range of 0−60 °C. The aspartic acid templating route produced titania nanospheres with relatively lower surface area (51 $m^2\ g^{-1}$).[28] The structure directing ability of these soft templates cannot be differentiated from the particle morphology of the titania materials, since, in each case, the resulting particles were uniform spherical in shape, although size of the particles vary from one template to another. Photocurrent generation was found to be directly related to the surface area of the titania material and, hence, on the templating agent. The salicylate-templated TiO_2, having a surface area of 176 $m^2\ g^{-1}$, produced a photocurrent (ΔI) of 7.6×10^{-7} for the RB-entrapped mesoporous TiO_2 sample, whereas for TiO_2, it was only 1.1×10^{-7} A.[22] Our results showed a very minor decrease in photocurrent (0.74×10^{-6} A) for the RB-entrapped crystalline mesoporous titania materials obtained via alginate templating pathway, while the corresponding photogenerated current in the absence of dye is 3.27×10^{-8} A.

CONCLUSIONS

The above experimental results prompted us to conclude that self-assembled mesoporous spherical TiO_2 nanoparticles can be synthesized by using a biopolymer sodium alginate as a template under different synthesis temperatures. The alginate biopolymer unit containing CO_2^- can be ligated to the positively charged Ti(IV) centers through covalent interaction, and hydrogen-bonding interactions between the alcoholic −OH groups facilitate to form the supramolecular structure of alginate moieties during the nucleation of particles, which, upon calcinations,

dx.doi.org/10.1021/am201759w | ACS Appl. Mater. Interfaces 2012, 4, 1560−1564

generates mesopores with dimensions of ~8−11.6 nm, depending on the synthesis conditions. These self-assembled TiO_2 nanoparticles exhibited high surface areas than the corresponding non-templated materials synthesized under similar pH conditions. The material with the greatest surface area showed drastic enhancement in the photoconductivity on entrapping an organic photosensitizer dye molecule (Rose Bengal) at its nanopores and, thus, the doping of the dye molecule enhances the photon-to-electron conversion process significantly.

■ ASSOCIATED CONTENT

Ⓢ Supporting Information

Additional figures and a table. This material is available free of charge via the Internet at http://pubs.acs.org.

■ AUTHOR INFORMATION

Corresponding Author

*Tel.: (+) 91-011-27666646. Fax: (+) 91-011-27667794. E-mails: basudebs@chemistry.du.ac.in (B.S.), msab@iacs.res.in (A.B.).

Notes

The authors declare no competing financial interest.

■ ACKNOWLEDGMENTS

B.S. is grateful to the University Grant Commission (UGC), India for financial support and University of Delhi. S.D. thanks UGC, India for a D.S. Kothari Postdoctoral Fellowship. S.D. thanks UGC, India for a junior research fellowship. A.K.P. thanks CSIR, India for a senior research fellowship. AB wishes to thank DST, New Delhi for providing instrumental facility through DST Unit on Nanoscience.

■ REFERENCES

(1) Wu, J. J.; Lu, X. J.; Zhang, L. L.; Huang, F. Q.; Xu, F. F. *Eur. J. Inorg. Chem.* **2009**, 2789−2795.

(2) Yang, S. C.; Yang, D. J.; Kim, J.; Hong, J. M.; Kim, H. G.; Kim, I. D.; Lee, H. *Adv. Mater.* **2008**, *20*, 1059−1064.

(3) Lu, X. J.; Mou, X. L.; Wu, J. J.; Zhang, D. W.; Zhang, L. L.; Huang, F.; Xu, F. F.; Huang, S. M. *Adv. Funct. Mater.* **2010**, *20*, 509−515.

(4) Luo, M.; Cheng, K.; Weng, W. J.; Song, C. L.; Du, P. Y.; Shen, G.; Han, G. R. *Nanoscale Res. Lett.* **2009**, *4*, 809−813.

(5) Araujo, P. Z.; Luca, V.; Bozzano, P. B.; Bianchi, H. L.; Arturo Soler-Illia, G. J. D. A.; Blesa, M. A. *ACS Appl. Mater. Interfaces* **2010**, *2*, 1663−1673.

(6) Li, H. X.; Bian, Z. F.; Zhu, J.; Die, D. Q.; Li, G. S.; Huo, Y. N.; Li, H.; Lu, Y. F. *J. Am. Chem. Soc.* **2007**, *129*, 8406−8407.

(7) Lee, S.-H. A.; Abrams, N. M.; Hoertz, P. G.; Barber, G. D.; Halaoui, L. I.; Mallouk, T. E. *J. Phys. Chem. B* **2008**, *112*, 14415−14421.

(8) Zhang, Y.; Xie, Z.; Wang. *ACS Appl. Mater. Interfaces* **2009**, *1*, 2789−2795.

(9) Das, S. K.; Bhunia, M. K.; Bhaumik, A. *Dalton Trans.* **2010**, *39*, 4382−4390.

(10) Hoffmann, M. R.; Martin, S. T.; Choi, W. Y.; Bahnemann, D. W. *Chem. Rev.* **1995**, *95*, 69−96.

(11) Epifani, M.; Diaz, R.; Arbiol, J.; Comini, E.; Sergent, N.; Pagnier, T.; Siciliano, P.; Taglia, G.; Morante, J. R. *Adv. Funct. Mat.* **2006**, *16*, 1488−1498.

(12) Skorb, E. V.; Shchukin, D. G.; Moehwald, H.; Sviridov, D. V. *J. Mater. Chem.* **2009**, *19*, 4931−4937.

(13) Liu, Z. Y.; Zhang, X. T.; Nishimoto, S.; Murakami, T.; Fujishima, A. *Environ. Sci. Technol.* **2008**, *42*, 8547−8551.

(14) Hartmann, P.; Lee, D. K.; Smarsly, B. M.; Janek, J. *ACS Nano* **2010**, *4*, 3147−3154.

(15) Long, M. C.; Beranek, R.; Cai, W. M.; Kisch, H. *Electrochim. Acta* **2008**, *53*, 4621−4626.

(16) Pal, N.; Paul, M.; Bera, A.; Basak, D.; Bhaumik, A. *Anal. Chim. Acta* **2010**, *674*, 96−101.

(17) Kresge, C. T.; Leonowicz, M. E.; Roth, W. J.; Vartuli, J. C.; Beck, J. S. *Nature* **1992**, *359*, 710−712.

(18) Goto, Y.; Inagaki, S. *Chem. Commun.* **2002**, 2410−2411.

(19) Meynen, V.; Cool, P.; Vansant, E. F. *Microporous Mesoporous Mater.* **2009**, *125*, 170−223.

(20) Mitra, A.; Bhaumik, A.; Imae, T. *J. Nanosci. Nanotechnol.* **2004**, *4*, 1052−1055.

(21) Liu, J.; Liu, F.; Gao, K.; Wu, J. S.; Xue, D. F. *J. Mater. Chem.* **2009**, *19*, 6073−6084.

(22) Patra, A. K.; Das, S. K.; Bhaumik, A. *J. Mater. Chem.* **2011**, *21*, 3925−3930.

(23) Xu, P.; Xu, T.; Lu, J.; Gao, S.; Hosmane, N. S.; Huang, B.; Dai, Y.; Wang, Y. *Energy Environ. Sci.* **2010**, *3*, 1128−1134.

(24) Zheng, Z.; Huang, B.; Qin, X.; Zhang, X.; Dai, Y. *Chem.−Eur. J.* **2010**, *16*, 11266−11270.

(25) Inaba, R.; Fukahori, T.; Hamamoto, M.; Ohno, T. *J. Mol. Catal. A: Chem.* **2006**, *260*, 247−254.

(26) Wang, Y. D.; Zhou, A. N.; Yang, Z. Y. *Mater. Lett.* **2008**, *62*, 1930−1932.

(27) Zhang, Z.; Zuo, F.; Feng, P. *J. Mater. Chem.* **2010**, *20*, 2206−2212.

(28) De, S.; Dutta, S.; Patra, A. K.; Bhaumik, A.; Saha, S. *J. Mater. Chem.* **2011**, *21*, 17505−17510.

(29) Schnepp, Z.; Wimbush, S. C.; Mann, S.; Hall, S. R. *CrystEngComm* **2010**, *12*, 1410−1415.

(30) Said, A. A.; Hassan, R. M. *Polym. Degrad. Stab.* **1993**, *39*, 393−397.

(31) Tada, H.; Kiyonaga, T.; Naya, S. *Chem. Soc. Rev.* **2009**, *38*, 1849−1858.

(32) Park, J. H.; Kim, S.; Bard, A. J. *Nano Lett.* **2006**, *6*, 24−28.

(33) Mitra, A.; Bhaumik, A.; Nandi, M.; Mondal, J.; Roy, B. K. *J. Solid State Chem.* **2009**, *182*, 1200−1205.

(34) Ma, T. Y.; Wei, Y. S.; Ren, T. Z.; Liu, L.; Guo, Q.; Yuan, Z. Y. *ACS Appl. Mater. Interfaces* **2010**, *2*, 3563−3571.

(35) Manga, K. K.; Wang, S.; Jaiswal, M.; Bao, Q.; Loh, K. P. *Adv. Funct. Mater.* **2010**, *22*, 5265−5270.

(36) Richter, C.; Schmuttenmaer, C. A. *Nat. Nanotechnol.* **2010**, *5*, 769−772.

(37) Aketagwa, K.; Hirama, H.; Moriguchi, H.; Torii, T. In *15th International Conference on Miniaturized Systems for Chemistry and Life Sciences*, October 2−6, 2011, Seattle, Washington, USA; pp 1615−1617.

(38) Li, C. J.; Xu, G. R. *Appl. Surf. Sci.* **2011**, *257*, 4951−4955.

(39) Zukalova, M.; Zukal, A.; Kavan, L.; Nazeeruddin, M. K.; Laska, P.; Gratzel, M. *Nano Lett.* **2005**, *5*, 1789−1792.

(40) O'Regan, B. B.; Durrant, J. R. *Acc. Chem. Res.* **2009**, *42*, 1799−1808.

(41) Ahmed, S.; Du Pasquier, A.; Birnie, D. P.; Asefa, T. *ACS Appl. Mater. Interfaces* **2011**, *3*, 3002−3010.

(42) Zhang, Z.-K.; Bai, -L.; Guo, D.-Z.; Hou, S.-M.; Zhang, G.-M. *Chem. Commun.* **2011**, *47*, 8439−8441.